# Scaled Model Aeroelastic Similarity of a Blended Wing Body through Multi-Disciplinary Optimization

Akshay Gupta

*MAE2 Aerospace Engineering, ISAE SUPAERO, Toulouse, France*

Joan Mas Colomer

*Post-PhD Candidate, ICA-ISAE SUPAERO, Toulouse, France*

Joseph Morlier

*Professor, ISAE SUAPERO-CNRS-INSA-Mines Albi-UPS, Toulouse, France*

## Declaration

This is to state that the present project (started February 1, 2018) is entirely my work. The theories and tools used in this project are given credit in this work and in the references. All literature used in this work is indicated in the bibliography placed at the end. It is confirmed that no sources have been used other than those stated.

I understand that plagiarism is a serious examination offence that may result in disciplinary action being taken.

Date: **March 28, 2019**

Signature: 

## Abstract

The work presented in this document is carried out under the course of mandatory Research Project for MSc in Aerospace Engineering at ISAE-SUPAERO. The work is based on the premise of previous works on aeroelastic scaling in the community, and optimization tools generated by Mas Colomer (ONERA) et al [1]. The aim of this work is to perform aeroelastic scaling on a Blended Wing Body (BWB) by making use of existing optimization-based design approach, and perform flutter optimization process thereafter. The work is divided into two semesters – S2, and S3. In S2, the aim is to thoroughly understand the concept of aeroelastic scaling, and apply it for two test cases – GOLAND Wing, and GARTEUR SM-AG19 model. In S3, the aim will be to perform aeroelastic scaling, and flutter optimization process for the BWB. The objective function is chosen so as to maximize similarity of modal parameters (i.e. modal shapes and frequencies) between the scaled model and the reference model, by optimizing structural properties of the given test case. These structural properties are the design variables for the optimization schedules. The verification of mode shape similarity is performed with Modal Assurance Criterion (MAC).

**Keywords:** Aeroelastic scaling, flutter, Blended Wing Body, modal shapes, modal frequencies, Modal Assurance Criterion.

## Nomenclature

| | |
|---|---|
| $\dot{(\cdot)}$ | Derivative with respect to time |
| $(^*)$ | Derivative with respect to nondimensional time |
| $\breve{(\ )}$ | Matrix with uniform dimensions |
| $\langle\ \rangle$ | Diagonal matrix |
| $\{\bar{\ }\}$ | Nondimensional Vector |
| $[\ ]^T$ | Transpose of a matrix |
| $[M]$ | Mass matrix |
| $[K]$ | Linearized stiffness matrix |
| $[T]$ | Transformation matrix |
| $\{a_g\}$ | Gravitational acceleration |
| $\{\eta\}$ | Vector of modal coordinates |
| $[\Phi]$ | Matrix of nondimensional mode shapes |
| $\omega$ | Modal frequency |
| $\tau$ | Nondimensional time |
| $\{x\}$ | Rigid body degrees of freedom vector |
| $r$ | Reference full scale model |
| $m$ | Scaled model |
| $b$ | Wing span |
| $c$ | Wing chord |
| $V$ | Airspeed |
| $N$ | Number of eigenpairs/extracted modes |
| $f$ | Objective function |
| $L$ | Length (any) considered for scaling |
| $E$ | Young's Modulus |
| $\nu$ | Poisson ratio |
| $\rho$ | Structural Density |
| $\lambda$ | Ratio (any) between scaled model and reference |
| $Fr$ | Froude Number |
| $g$ | Gravitational acceleration |
| $\mu$ | Inertia ratio |
| $S$ | Wing area |
| $m\_c$ | Concentrated point mass |
| $t$ | Membrane thickness |
| $t_{min}$ | Lower bound for thickness |
| $t_{max}$ | Upper bound for thickness |
| $\bar{t}$ | Normalized time |
| $t_0$ | Initial thickness design variable |
| $m_0$ | Initial concentrated mass design variable |
| $tol$ | Tolerance limit of the optimizer |
| BWB | Blended Wing Body |
| FE | Finite element |
| JWSC | Joined Wing SensorCraft |
| MAC | Modal Assurance Criterion |
| $MAC_{trace}$ | Trace of MAC matrix |
| LCO | Limit Cycle Oscillation |

## 1 Introduction

### 1.1 Motivations

In Aeronautics, it is a common practice to experimentally test aeroelastically scaled models to verify the predicted aeroelastic characteristics of the full scale vehicle. In some cases, the objective can only be to verify the computational models. For such cases, the scaled model needs to represent the full scale model, subjectively.

Flutter is a dynamic aeroelastic instability that can cause catastrophic failure during the flight. Hence, it is highly important to carry out flutter analysis. Taking inspiration from the past works in this field, and to unleash the new methods for the implementation of aeroelastic scaling, this work addresses the aeroelastic scaling and flutter optimization for two initial (GOLAND wing & GARTEUR SM-AG19) and one final test case (BWB).

### 1.2 Project Plan

The work is divided into two semesters S2, and S3. In first semester i.e. S2, the work comprises of reading existing literature on the concept of aeroelasticity, flutter, scaling theories, and optimization. The next step is to understand the concept of dynamic modal optimization and aeroelastic static scaling. The tools generated by Mas Colomer et al. [1] forms the basis of the implementation part of this work. It is highly important to make oneself familiar with those tools. OpenMDAO tutorials are also performed for several weeks. In the work for this semester, flow similarity is assumed between the scaled models and the full scale reference models. The work of this semester is concluded with the dynamic modal optimization of two test cases namely, GOLAND wing, and GARTEUR SM-AG19 model. Each test case is scaled for a scale of both greater than one and smaller than one.

In the second half i.e. S3, the main task would be to revise the aeroelastic static scaling, learn the theory of dynamic aeroelastic scaling, performing dynamic modal optimization of the BWB for scales greater and smaller than one, and flutter analysis and optimization for the reference BWB. In

this part of the work, there would be no flow similarity assumption, hence, it will an integral part of the work to maintain structure and aerodynamics in place. The flutter optimization will also be performed for scaled models of scales both greater and smaller than one. In the end, a research paper will be published with new findings and improvements on existing concepts, as seen throughout the course of this work.

### 1.3 Literature Review

The concept of aeroelastic scaling has been used since the early 60's and is based on the premise that the scaled model will present the same (almost) scaled aeroelastic response as the full scale target vehicle. The basis of all scaling theories is the non-dimensionalization of the system's governing equations of motion according to Buckingham's $\pi$–theorem [2]. In the early 60's, Bisplinghoff et al. first applied this scaling concept to the aeroelastic equations of motion in it Principles of Aeroelasticity [3] where they highlighted the importance of the matching of scaled stiffness and mass between the full scale model and the scaled models. However, not much investigation was done on the different scaling parameters and their influence on the scaled model aeroelastic response. A decade later, Wolowicz wrote *Similitude Requirements and Scaling Relationships as Applied to Model Testing* [4], an in-depth study on the influence of the different scaling parameters on the scaled aeroelastic response of the scaled model. With further developments into finite element analysis and computational tools, optimization of FE models became a possibility and the path towards aeroelastic scaling procedures converged.

Lately, there has been an increasing effort from the scientific community on the validation of different methodologies and assumptions used to aeroelastically scale a model through FE models optimization procedures. Pereira et al. [5] optimized both stiffness and mass distributions through the same optimization routine in order to match the scaled natural frequencies of the full-scale model. Richards et al. [6] (2010) and Eger et al. [7] [8] (2013) used two separate optimization routines in order to efficiently optimize the stiffness and mass distributions of the scaled model while matching the scaled natural frequencies and the non-dimensional mode shapes of the full-scale model with fairly good results. Bond et al. [9] (2012) added non-linear effects (buckling eigenvalues and mode shapes) to the two-step optimization routine previously stated however, the non-linear static response only matched up to 60% of the buckling load even though they proved the necessity of matching non-dimensional mode shapes in addition to the scaled natural frequencies in order to have a matching scaled aeroelastic response. Finally, Ricciardi [10] further developed Bond's research producing methods that closely replicate the target's non-linear aeroelastic behavior while identifying new sources of local optima.

A new methodology for designing nonlinear aeroelastically scaled models that uses direct matching of linear and nonlinear static responses to trim loads while simultaneously satisfying modal frequency constraints is studied by Ricciardi et al. [11] (2014). This was also the first scaling demonstration to include nonlinear aeroelastic verification. An equivalent static loads approach was used to transform the nonlinear static response to an equivalent linear system and facilitate efficient optimization with gradient-based methods. This paper is good to understand the basics of scaling the models, understanding the dynamic aeroelastic equation terms and significance.

Tiago [12], in his work performed two linear aeroelastic scaling analyses. First analysis was for a simple half-span rectangular Wingbox. The scaling procedure was based on the iterative optimization of a finite element model in order to have matching non-dimensional mode shapes and reduced frequencies between the full-scale model and the scaled models. The second analysis was for Boeing's Joined Wing SensorCraft. In this case, there was no structural similitude between full scale and scaled models due to lack of information as Boeing did not provide the prototype's internal structure. The data for stiffness matching with eight different load cases, and the modal analysis data for C.G. constrained and free modal response of the full scale JWSC for the first 30 vibration modes.

For the Wingbox case, there was a really good matching of the scaled aeroelastic response with the correct flutter mode, frequency and velocity being captured with both the 'g-method' and the 'K-method'. However, for the Joined Wing SensorCraft, even though the correct flutter mode and frequency were matched, there was a big disparity in terms of the flutter velocity with relative errors around 33% for both the 'g-method' and the 'K-method'. These big errors come from the fact that there was no structural similarity between the scaled and the full scale models which made the optimization procedure much more time-consuming and

with worse overall results than that of the Wingbox where the scaled model structure layout was previously defined. This fact proves the importance of using a structurally similar scaled model as the initial design point when aeroelastically scaling a prototype.

In 2016, Ricciardi et al. [13] presented improvements and additional works on their last paper. The method optimized an incremental number of vibration eigenpairs, buckling eigenpairs, and optionally a linear static response of scaled models to match the scaled values of a target full-scale aircraft. A method for matching scaled modal mass, a required scaling parameter, was developed. The sources of local optima were identified and a tiered global-search-optimization procedure was incorporated. The approach was demonstrated on a joined-wing scaled-model-design problem.

In 2017, Mas Colomer et al. [1], presented an optimization process capable of sizing a scaled flight demonstrator in order to reproduce several behaviors encountered on its corresponding full size aircraft. The main aim was to maximize the similarity between the scaled model and the full size aircraft. When flow similarity (e.g., same Mach number) does not exist between the model and the aircraft, the same scaled deformed shape cannot be obtained by simply scaling the stiffness and preserving of the outer mold line.

They presented the traditional scaled modal optimization and introduced the use of the Modal Assurance Criterion both for reordering the normal modes according to their shape and for the definition of the objective function. This method should avoid the discontinuities on the objective function and on the derivatives of the constraints.

## 1.3 Concept of Flutter

Flutter is the state of turbulent vibrations of a lifting surface in coupled bending and torsional direction which ultimately can lead to catastrophic failures and destruction of the whole airplane structure. When a lifting surface is placed in an unsteady fluid flow, it will experience disturbances over the surface area. These disturbances have a specific frequency at which they vibrate. At low initial speeds, the oscillations are damped by the structural stiffness. Hence, the oscillations does not go violent and are under control. This is a normal state and needs no special attention. As the fluid flow speed increases with respect to the lifting surface, the oscillation frequency increases and the rate of structural damping decreases gradually which results in a high but steady amplitude oscillations of the lifting surface. This state is called the Zero-damping state as the structural damping reduces to zero and this speed of fluid flow is called Critical flutter speed. At this state, an oscillation can just maintain itself with a steady amplitude. Above the critical flutter speed, a small disturbance in the fluid flow can trigger to initiate an oscillation of great violence. In other words, we can describe the flutter phenomenon is three stages. Stage I is when the speed is less than the critical flutter speed and the structural damping is positive, hence, the oscillations die out after a period of time. Stage II is when the speed is equal to the critical flutter speed and the structural damping is near to 0+ or 0 (zero). At this stage, the oscillations neither grow nor die, the lifting surface oscillates with a steady amplitude. Stage III is when the fluid flow speed becomes more than the critical flutter speed and the structural damping becomes negative, so as to support the oscillations to become more violent. This state is called flutter and its analysis is the main objective of this work.

There is more than one reason for the occurrence of flutter. Flutter phenomenon is also a result of coupling of several degrees of freedom, which is also an essential feature of flutter. The past experiments proves that most of the times the bending deformations across the span are in phase with one another. Similarly, the torsional movements across the span are in phase, but the bending is significantly out of phase from the torsional deformation. This phase difference is responsible for occurrence of the flutter phenomenon. An airplane wing, as a deformable elastic body, has infinitely many degrees of freedom. But we can describe the airplane's elastic deformation in any chordwise section using only two degrees of freedom with sufficient accuracy: the vertical deflection at any reference point and the angle of rotation of a point, i.e., the bending and torsional deformations, respectively.

Non-linearity in flutter exists due to two reasons, Aerodynamics and Structure. Stall flutter (when the flow separates from the boundary layer) is the aerodynamic non-linearity whereas the Limit Cycle Oscillation (LCO) is the structural non-linearity. LCO is the bounded motion of the

lifting surface with high amplitudes, the amplitude does not increase after a certain speed but the oscillation persists and the lifting surface vibrates laterally and torsionally with a high amplitude. The motion is controlled and the LCO resembles a closed loop system.

Nowadays, Flutter speed/frequency is a necessary flight characteristic for airplane certification for it provides an estimation for the airplane's maximum operational speed, often designated as dive speed.

## 2 Methodology

### 2.1 Scaling Theory

Scaling theory is developed based on the geometrically nonlinear dynamic aeroelastic equation of motion [11],

$$[M]\{\ddot{x}\} + [K_{NL}(x)]\{x\} = [A_k]\{x\} + [A_c]\{\dot{x}\} + [A_m]\{\ddot{x}\} + [M]\{a_g\} \quad (1)$$

where $\{x\}$ is a vector of elastic and rigid body degrees of freedom, $[M]$ is the mass matrix (a function of $\{x\}$ due to nonlinear kinematics), $[A_k]$, $[A_c]$, and $[A_m]$ are aerodynamic matrices, and $\{a_g\}$ is a vector containing gravitational accelerations for each degree of freedom. $(\dot{})$ indicates differentiation with respect to time. Nonlinear kinematics don't introduce different physical quantities than those needed for compatible linear and geometrically nonlinear formulations. There are, however, possible issues with existing scaled model design methodologies that were originally developed for applications with essentially linear kinematics. For the purpose of linearized dynamic aeroelastic equation of motion,

$$[M]\{\ddot{x}\} + [K]\{x\} = [A_k]\{x\} + [A_c]\{\dot{x}\} + [A_m]\{\ddot{x}\} + [M]\{a_g\} \quad (2)$$

where $[K]$ is the linearized stiffness matrix. For Eqn. (2) to be nondimensionalized, the components of each coefficient matric must have unified dimensions. Coefficient matrix dimensions are unified using a dimensional transformation matrix, $[T]$ that is derived to nondimensionalize the physical coordinate vector. For instance, if the physical coordinates are two displacement and two rotation degrees of freedom,

$$\{x\} = \begin{Bmatrix} h_1 \\ \theta_1 \\ h_2 \\ \theta_2 \end{Bmatrix} \quad (3)$$

Then a nondimensional vector of physical coordinates $\{\bar{x}\}$ is attained using,

$$\{x\} = [T]\{\bar{x}\} = \begin{bmatrix} b & 0 & 0 & 0 \\ 0 & 1 & 0 & 0 \\ 0 & 0 & b & 0 \\ 0 & 0 & 0 & 1 \end{bmatrix} \begin{Bmatrix} h_1/b \\ \theta_1 \\ h_2/b \\ \theta_2 \end{Bmatrix} = \begin{Bmatrix} h_1 \\ \theta_1 \\ h_2 \\ \theta_2 \end{Bmatrix} \quad (4)$$

(Refer to *Appendix A* to get an insight on finding similarity parameters.)

The coefficient matrices are uniformly dimensionalized by premultiplying by $[T]^T$ and postmultiplying by $[T]$. Take the mass matrix for example,

$$[\breve{M}] = [T]^T[M][T] \quad (5)$$

where $\breve{(\ )}$ denotes a matrix or vector with uniform dimensions. Gravitational acceleration is modified similarly,

$$\{a_g\} = [T]\{\breve{a}_g\} \quad (6)$$

Eqn. (2) is uniformly dimensionalized by substituting for {x} and $\{a_g\}$ with the general forms of Eqns. (4) and (6) and premultiplying by $[T]^T$.

$$[\breve{M}]\{\ddot{\bar{x}}\} + [\breve{K}]\{\bar{x}\} = [\breve{A_k}]\{x\} + [\breve{A_c}]\{\dot{\bar{x}}\} + [\breve{A_m}]\{\ddot{\bar{x}}\} + [\breve{M}]\{\breve{a}_g\} \quad (7)$$

Each term in Eqn. (7) has units of work, or force × length. Nondimensional deformations in terms of the modal coordinates are

$$\{\bar{x}\} = [\Phi]\{\eta\} \quad (8)$$

where $\{\eta\}$ is the vector of modal coordinates and $[\Phi]$ is the matrix of nondimensional mode shapes. The first six mode shapes are rigid body displacements. Mass and stiffness matrices are diagonalized using the bi-orthogonality property,

$$\langle m \rangle = [\Phi]^T [\breve{M}][\Phi] \tag{9}$$

$$\langle k \rangle = [\Phi]^T [\breve{K}][\Phi] = \langle m\omega^2 \rangle \tag{10}$$

where $\langle \omega \rangle$ is the diagonal matrix of modal frequencies. Aerodynamic coefficient matrices are modified equivalently,

$$[a_k] = [\Phi]^T [\widetilde{A_k}][\Phi] \tag{11}$$

$$[a_c] = [\Phi]^T [\widetilde{A_c}][\Phi] \tag{12}$$

$$[a_m] = [\Phi]^T [\widetilde{A_m}][\Phi] \tag{13}$$

Using modal coordinates, the equation of motion is,

$$\langle m \rangle \{\ddot{\eta}\} + \langle m\omega^2 \rangle \{\eta\} = [a_k]\{\eta\} + [a_c]\{\dot{\eta}\} + [a_m]\{\ddot{\eta}\} + \langle m \rangle [\Phi^{-1}]\{\widetilde{a_g}\} \tag{14}$$

After:

1. Moving the dimensions of aerodynamic matrices and gravitational acceleration vector outside as scalar coefficients,
2. Nondimensionalising the mass using m1, modal mass (uniformly distributed as inertia) of the first mode,
3. Nondimensionalising the time using ω1, the modal frequency of the first mode,
4. Rearranging and writing in the form of three nondimensional parameters which emerge in the equation namely: reduced frequency of the first elastic mode $k_{red\_1} = \frac{\omega_1 b}{V}$, inertia ratio $\mu_1 = \frac{\rho S b(b^2)}{m_1}$, and Froude number $Fr = \frac{V}{\sqrt{bg}}$. Froude number is not a universally required scaling parameter but it is required when the gravitational term is considered.

The final form of the nondimensional linear aeroelastic equation is,

$$\langle \bar{m} \rangle \{\eta^{**}\} + \langle \bar{m}\bar{\omega}^2 \rangle \{\eta\} = \frac{1}{2}\frac{\mu_1}{{K_1}^2}([\overline{a_k}]\{\eta\} + K_1[\overline{a_c}]\{\eta^*\} + {K_1}^2[\overline{a_m}]\{\ddot{\eta}\}) + \frac{1}{Fr^2 {K_1}^2}\langle \bar{m} \rangle [\Phi^{-1}]\{\overline{a_g}\} \tag{15}$$

where:

1. (*) indicates differentiation with respect to nondimensional time $\tau = t\omega_1$,
2. $\langle \bar{m} \rangle$ is a diagonal matrix of nondimensional masses with $\overline{m_1} = 1$, and
3. $\langle \bar{\omega} \rangle$ is a diagonal matrix of nondimensional modal frequencies

For the scaled model to have a scaled linearized dynamic aeroelastic response, as governed by Eqn. (15), the following derived nondimensional parameters are required to match the full scale model:

1. Reduced frequency of the 1st mode $k_{red\_1}$,
2. Inertia ratio $\mu_1$,
3. Froude number $Fr$,
4. Nondimensional modal mass $\langle \bar{m} \rangle$,
5. Nondimensional modal frequencies $\langle \bar{\omega} \rangle$,
6. Nondimensional modal shapes $[\Phi]$,
7. Aerodynamic shape,
8. Mach number if compressibility effects are taken into account, and
9. Reynolds number if viscous effects are taken into account

## 2.2 Optimizer Objective Function

The traditional scaled model optimization as presented by Ricciardi et al. [11] proposed an objective function which minimized the difference between the mode shapes of the full scale model and the scaled model as defined in Eqn. (16).

$$\sum_{i=1}^{N} \left\| \{\bar{\Phi}\}_{r,i} - \{\bar{\Phi}\}_{m,i} \right\| \tag{16}$$

where $\{\bar{\Phi}\}_{r,i}$ is the $i^{th}$ normalized mode shape of the reference full scale model, $\{\bar{\Phi}\}_{m,i}$ is the $i^{th}$ normalized mode shape of the scaled model, and $N$ is the number of eigenpairs.

The problem was constrained so as to match the reduced frequencies, as defined in Eqn. (17).

$$\omega_{r,i} = \omega_{m,i} \Rightarrow \frac{b_r}{V_r} = \frac{b_m}{V_m} \quad , \quad i = 1, 2, \dots, N \tag{17}$$

where the subscript $r$ indicates the reference full scale model, subscript $m$ indicates the scaled model, $b$ indicates the wingspan, and $V$ is the airspeed.

The normal modes are sorted according to the increasing values of their corresponding frequencies. However, as mentioned in Section 1.2, Mas Colomer et al. [1] pointed out that the drawback of such an approach is the introduction of discontinuities in the objective function and on the derivatives of the constraints as defined in Eqns. (16) and (17), respectively. They proposed to compare modes after sorting them according to the nature of their respective shape. The modes can be reordered to find the similarity between the mode shape of an iteration and the mode shape of the target model. This can be repeated for all mode shapes of the target model. To achieve this, they introduced an optimization formulation that can track the modes using Modal Assurance Criterion (MAC), which is a value that quantifies how similar the two modes are. The MAC between any two mode shapes $\Phi_1$ and $\Phi_2$ is defined as the normed scalar product between the two vectors [14], as defined in Eqn. (18).

$$MAC(\Phi_1, \Phi_2) = \frac{\left\|\Phi_1^T \Phi_2\right\|}{(\Phi_1^T \Phi_1)(\Phi_2^T \Phi_2)} \tag{18}$$

From Eqn. (18), we can conclude that,

$$MAC = \begin{matrix} 1, & consistent\ modes \\ 0, & non-consistent\ modes \end{matrix}$$

It is proposed to create a matrix of MAC values for all the modes that are tracked between the reference full scale model and the scaled model, and sort them by comparing their MAC values (closest to one). The trace of this sorted MAC matrix should ideally be equal to $N$, which is the case when there is perfect matching between the modes of reference and scaled model.

In this work, the objective is to achieve the value of trace of MAC matrix as close as possible to $N$. **The objective function is to minimize the function as defined in Eqn. (19).** For the ideal matching, the value of $f$ should converge to zero.

$$f = \frac{N - MAC\_trace}{N} \tag{19}$$

where $N$ is the number of modes to consider for comparison out of total $M$ extracted modes.

## 2.3 Working of Modal Optimization Algorithm

The tools developed by Mas Colomer et al. are used to perform the modal optimization. The working of the tools is based on the idea as described in Section 2.2.

The tools consist of a main program which calls different classes, OpenMDAO directories, and NASTRAN extensions. In this work, the design variables of the optimization schedules are chosen concerning **only** the modal similarity. **The hypothesis of flow similarity between the reference full scale model and the scaled model is active.** This will not be the case in the second half of this work, since in that case the flutter response of each scale will be compared and corrections in the aerodynamic models according to the parameters of each scale (Mach, Reynolds ...) will be made.

In this work, the design variables are the membrane thicknesses, and the concentered masses. The normal working of the code is to alter the design variables within the applied bounds, and optimize for the objective function as defined in Eqn. (18) until the specified tolerance is reached. As a result, the optimum values for membrane thicknesses and concentrated masses for which the reference and scaled models are aeroelastically similar, are obtained. The optimization schedule is represented in **Figure 1.**

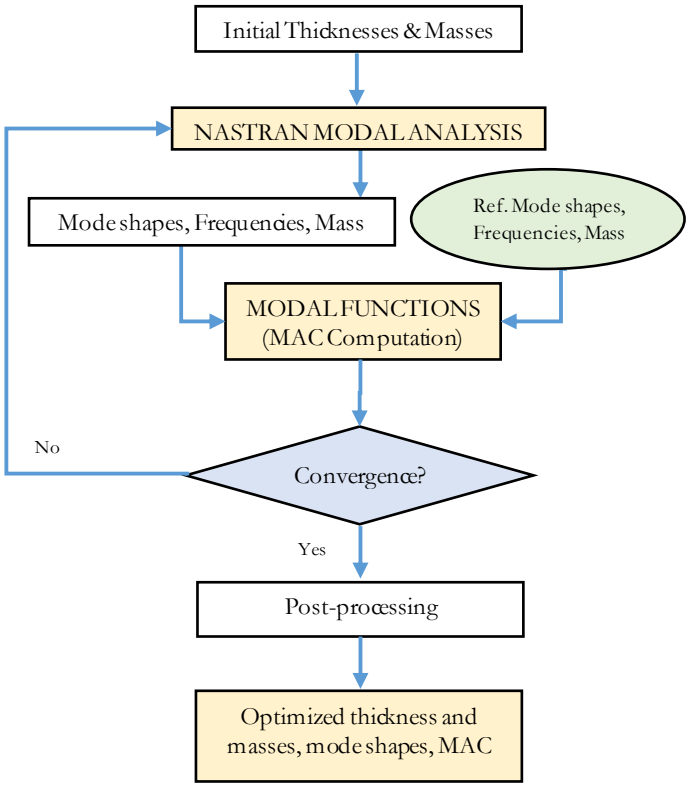


**Figure 1:** *Optimization Methodology*

# 3 Test Cases

## 3.1 GOLAND Wing

### 3.1.1 General Description

The GOLAND wing used as the first test case is a rectangular cantilevered wing, without a tip store, with a 20ft span ($b_r = L_r$), and 4ft chord $c_r$. The airfoil consists of a 4% thick parabolic curve. The wing is equipped with 10 concentrated point masses, represented with black dots as shown in **Figure 2.**

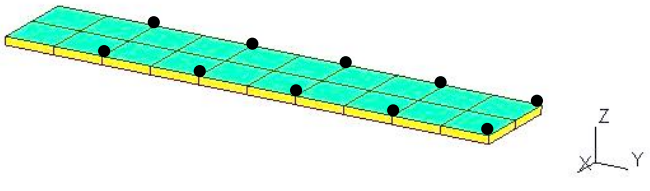


**Figure 2:** *GOLAND Wing Geometry*

The material properties for this test case are defined in **Table 1.**

**Table 1:** *Material Properties for GOLAND wing*

| **Property** | English Units | Metric Units |
|---|---|---|
| **E** | $1.4976 \times 10^9$ psf | $71705\ MPa$ |
| **ν** | 0.33 | 0.33 |
| **ρ** | $1 \times 10^{-4}$ slugs/ft$^3$ | $0.0515\ kgm^{-3}$ |

### 3.1.2 Aeroelastic Scaling Parameters Calculation

The following procedure is followed to get scaling ratios for the parameters required for this work.

**Recall:** Flow similarity hypothesis is active!

**Step I:** Select a length ratio,

$$\lambda_L = \frac{L_m}{L_r} \tag{20}$$

**Step II:** For frequency ratio $\lambda_\omega$,

Flow similarity implies that Froude number $Fr$ is same for the reference $(r)$ and the scaled model $(m)$,

$$Fr = \frac{V_m}{\sqrt{b_m g}} = \frac{V_r}{\sqrt{b_r g}}$$

$$\lambda_V = \frac{V_m}{V_r} = \sqrt{\frac{L_m}{L_r}}$$

Taking into account the reduced frequency, $k_{red} = \frac{b\omega}{V}$

$$\left(\frac{b\omega}{V}\right)_m = \left(\frac{b\omega}{V}\right)_r$$

$$\lambda_\omega = \frac{\omega_m}{\omega_r} = \frac{V_m}{V_r} \times \frac{L_r}{L_m} \tag{21}$$

**Step III:** For mass ratio $\lambda_M$,

$$\mu = \left(\frac{\rho S b}{M}\right)_m = \left(\frac{\rho S b}{M}\right)_r$$

where $S = bc$, $b = L$, and $c_m = \frac{L_m}{L_r} \times c_r$

simplifying, we get, $\lambda_M = \frac{M_m}{M_r} = \left(\frac{L_m}{L_r}\right)^3 = (\lambda_L)^3$ (22)

From Eqns. (20), (21), and (22), for three length (span) ratios, the frequency and mass ratios are calculated and listed in **Table 2**.

**Table 2:** *Scaling Ratios for GOLAND wing*

| Sub-case | $\lambda_L$ | $\lambda_\omega$ | $\lambda_M$ |
|---|---|---|---|
| **I** | 1/4 | 2 | 1/64 |
| **II** | 1/9 | 3 | 1/729 |
| **III** | 4 | 1/2 | 64 |

## 3.2 GARTEUR SM–AG19

### 3.2.1 General Description

The GARTEUR SM–AG19 model presented by Link and Friswell [15], is shown in **Figure 3.** The model is equipped with three concentrated point masses at the wing tips and empennage, represented by black dots. The full wing span is 2000 mm $(b_r = L_r)$. The model is not constrained, hence, the first six modes from NASTRAN modal analysis would be rigid body modes and should not be taken into consideration.

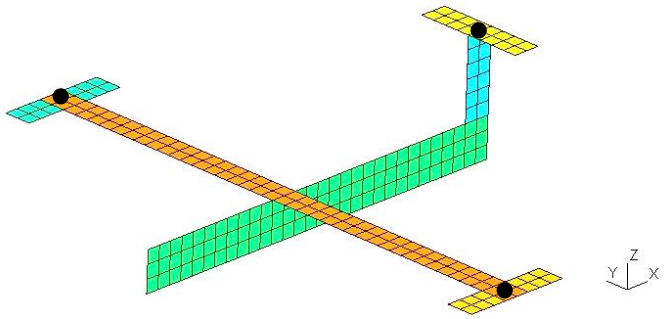


**Figure 3:** *GARTEUR SM-AG19 Geometry*

The material properties are defined in **Table 3.**

**Table 3:** *Material Properties for GARTEUR SM-AG19*

| Property | English Units | Metric Units |
|---|---|---|
| **E** | $1.5 \times 10^9$ psf | $72000\ MPa$ |
| **ν** | 0.33 | 0.33 |
| **ρ** | $5.24 \times 10^{-9}$ slugs/ft³ | $2.7 \times 10^{-6}\ kgm^{-3}$ |

### 3.2.2 Aeroelastic Scaling Parameters Calculation

The calculations and derivations mentioned in Section 3.1.2 are followed for this test case.

From Eqns. (20), (21), and (22), for three length (span) ratios, the frequency and mass ratios are calculated and listed in **Table 4**.

**Table 4:** *Scaling Ratios for GARTEUR SM-AG19*

| Sub-case | $\lambda_L$ | $\lambda_\omega$ | $\lambda_M$ |
|---|---|---|---|
| **I** | 1/9 | 3 | 1/729 |
| **II** | 2 | 5/7 | 8 |

# 4 Modal Optimization Formulation

## 4.1 Initial Value of Design Variables

To avoid the start from a completely blind point, in dynamic scaling, the initial values of design variables can be estimated by a thumb rule, which gives good starting points to the optimizer. The quick estimation rule states that the concentrated mass values for a scaled model with mass ratio $\lambda_M$ can be estimated taking into account the $\lambda_M$ ratio. Similarly, for the membrane thickness values for a scaled model with length ratio $\lambda_L$ can be estimated by taking the square of the $\lambda_L$ ratio. Eqns. (23), and (24) show the relationship mathematically.

$$\lambda_{m\_c} = \frac{m\_c_m}{m\_c_r} \cong \frac{M_m}{M_r} = \lambda_M \tag{23}$$

$$\lambda_t = \frac{t_m}{t_r} \cong \left(\frac{L_m}{L_r}\right)^2 = \lambda_L \tag{24}$$

where $m\_c$ represents concentrated point mass, and $t$ represents membrane thickness.

## 4.2 About the Optimizer

The Constrained Optimization by Linear Approximation (COBYLA) optimizer is used for all the test cases. It is a method for constrained problems where the derivative of the objective function is not known. It does not need to know the gradient of the objective function, as it can find a vector that has minimal (or maximal) $f$, the objective. However, it must be taken care of in terms of bounds. The COBYLA optimizer can go out of bounds quickly, and hence, the values for upper and lower bounds for the design

variables are to be chosen carefully. For example, the COBYLA optimizer can produce negative thicknesses, which are not accepted by NASTRAN, it will display an error in that case. The reason for it going to negative values can be very low value of bound in comparison with the 'rhobeg' of the optimizer. The COBYLA optimizer can be imagined to work with a sphere of radius 'rhobeg', which takes same step in both forward and backward direction on a normalization scale.

Let's say for thickness $t$ as design variable with bounds $t_{max}$ and $t_{min}$, the normalization would be as depicted in Eqn. (25).

$$\bar{t} = \frac{t - t_{min}}{t_{max} - t_{min}} \tag{25}$$

If $t_{min}$ is too small, the optimizer can go very close to $\bar{t} = 0$. Near $\bar{t} = 0$, if 'rhobeg' is larger than the distance between current $\bar{t}$ and zero, the optimizer will take a negative value. This is illustrated in **Figure 4.**

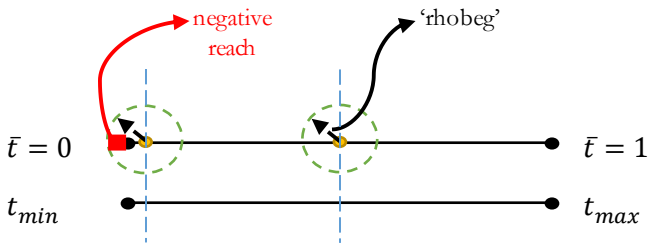


**Figure 4:** *Negative value problem with COBYLA Optimizer*

An alternative method to tackle the problem of negative thicknesses is to normalize each design variable individually instead of normalizing one type of design variable altogether. Which is to say, all thicknesses should be normalized individually depending on their initial value. Similarly, all the concentrated point masses shall be normalized individually.

All the test cases presented in this work have some optimization formulation in common. Those are listed in **Table 5.**

**Table 5:** *Common Formulation for All Test Cases*

| | |
|---|---|
| **Objective function** | $\boldsymbol{f = min\left(\frac{N - MAC\_trace}{N}\right)}$ |
| **Design Variables** | Membrane thicknesses & Concentrated Masses vectors |
| **Constraints** | Reduced frequency matching, Eqn. (21)<br>Mass matching, $M_m - M_r = 0$ |
| **Number of Extracted Modes** | $N = 5$ |

## 4.3 Test Cases – GOLAND Wing

Three sub-cases are performed for GOLAND wing, as mentioned in **Table 2.** The optimization formulation for each sub-case is detailed in **Table 6, 7,** and **8.**

**Table 6:** *Sub-case I Optimization Formulation*

| | |
|---|---|
| **Scaling Ratio** | $\boldsymbol{\lambda_L = \frac{1}{4}}$ |
| **Initial Value of Design Variables** | $t_0 = \frac{1}{16} \times t_{ref}, m_o = \frac{1}{64} \times m_{ref}$ |
| **Bounds** | $t_0$:$[4 \times 10^{-5}, 6 \times 10^{-3}]$<br>$m_0$:$[2 \times 10^{-2}, 9 \times 10^{-2}]$ |
| **Tolerance** | $tol = 1 \times 10^{-3}$ |
| **Iterations** | max = 200<br>actual = 77 |

**Table 7:** *Sub-case II Optimization Formulation*

| | |
|---|---|
| **Scaling Ratio** | $\boldsymbol{\lambda_L = \frac{1}{9}}$ |
| **Initial Value of Design Variables** | $t_0 = \frac{1}{81} \times t_{ref}, m_o = \frac{1}{729} \times m_{ref}$ |
| **Bounds** | $t_0$:$[7.5 \times 10^{-5}, 1.4 \times 10^{-3}]$<br>$m_0$:$[1.35 \times 10^{-3}, 7.32 \times 10^{-3}]$ |
| **Tolerance** | $tol = 1 \times 10^{-3}$ |
| **Iterations** | max = 500<br>actual = 155 |

**Table 8:** *Sub-case III Optimization Formulation*

| Scaling Ratio | $\lambda_L = 4$ |
|---|---|
| Initial Value of Design Variables | $t_0 = 16 \times t_{ref}, m_o = 64 \times m_{ref}$ |
| Bounds | $t_0 : [0.1 \times t_0 , 5 \times t_0]$<br>$m_0 : [63 , 341]$ |
| Tolerance | $tol = 1 \times 10^{-3}$ |
| Iterations | max = 200<br>actual = 200 |

Note that in Sub-case III, we are normalizing bounds for thicknesses individually. This alternative was sought after the main program resulted in negative thicknesses.

### 4.4 Test Cases – GARTEUR SM-AG19

Two subcases are performed for GARTEUR model, as mentioned in **Table 3.** The model is not constrained, so 'free_free' is set to 'True'. 'free_free' is a depiction used in the main optimization tool, to identify if the model has rigid body modes or not. The optimization formulation for sub-case I and II is detailed in **Table 8, and 9.**

**Table 8:** *Sub-case I Optimization Formulation*

| Scaling Ratio | $\lambda_L = \frac{1}{9}$ |
|---|---|
| Initial Value of Design Variables | $t_0 = \frac{1}{81} \times t_{ref}, m_o = \frac{1}{729} \times m_{ref}$ |
| Bounds | $t_0 : [1 \times t_0 , 100 \times t_0]$<br>$m_0 : [0.01 \times m_0 , 1 \times m_0]$ |
| Tolerance | $tol = 1 \times 10^{-8}$ |
| Iterations | max = 500<br>actual = 247 |

Multiple number of iterations were performed to obtain the optimized results. They include increase in number of iterations, increase/decrease of bounds, individual/group normalizing of design variables bounds, and increasing tolerance. We find that, for subcase I, increasing tolerance from 1e-3 to 1e-8, improved the objective function result drastically. The bounds were so chosen as to produce least error in the values of frequencies and masses for the scaled model.

**Table 9:** *Sub-case II Optimization Formulation*

| Scaling Ratio | $\lambda_L = 2$ |
|---|---|
| Initial Value of Design Variables | $t_0 = 4 \times t_{ref}, m_o = 8 \times m_{ref}$ |
| Bounds | $t_0 : [0.2 \times t_0 , 20 \times t_0]$<br>$m_0 : [0.002 \times m_0 , 0.2 \times m_0]$ |
| Tolerance | $tol = 1 \times 10^{-15}$ |
| Iterations | max = 500<br>actual = 277 |

## 5 Results of Scaling

The results for all the sub-cases for both the test cases are listed in this section. The important results include frequency matching, concentrated mass matching, sorted MAC matrix, and convergence graphs. The results are listed in a chronological order.

### 5.1 GOLAND Wing

#### 5.1.1 Sub-case I: $\lambda_L = \frac{1}{4}$

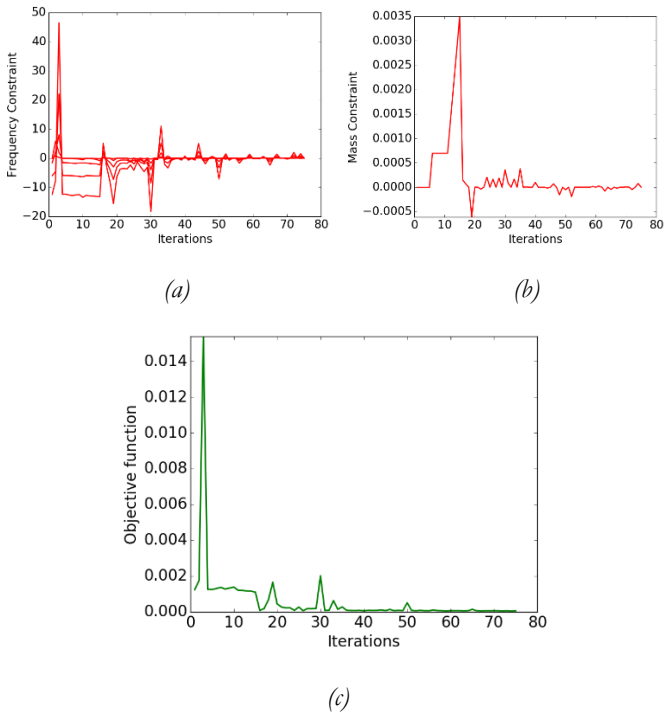


*(a)* *(b)*

*(c)*

**Figure 5:** *Convergence Graphs (all bounds normalized together): (a) Frequency Constraint, (b) Mass Constraint, (c) Objective Function*

**Table 10:** *Modal Response Matching for first 5 modes*

| Mode | Reference Value | Target Value | Optimized Value | Error% |
|---|---|---|---|---|
| **1** | 2.40 | 4.794 | 4.795 | 8e-3 |
| **2** | 8.65 | 17.301 | 17.300 | 3e-3 |
| **3** | 13.22 | 26.445 | 26.446 | 5e-3 |
| **4** | 15.94 | 31.887 | 31.890 | 1e-2 |
| **5** | 24.11 | 48.228 | 48.228 | 1e-4 |
| **Mass (slugs)** | 32.871 | 0.51 | 0.51 | 5e-5 |

$$\begin{bmatrix} 1.00 & 0.24 & 0.00 & 0.00 & 0.04 \\ 0.24 & 1.00 & 0.03 & 0.01 & 0.04 \\ 0.00 & 0.03 & 1.00 & 0.00 & 0.11 \\ 0.00 & 0.01 & 0.00 & 1.00 & 0.00 \\ 0.04 & 0.04 & 0.11 & 0.00 & 1.00 \end{bmatrix}$$

**Matrix 1:** *Modal Assurance Criterion Matrix to ensure Mode Shape matching for first five modes*

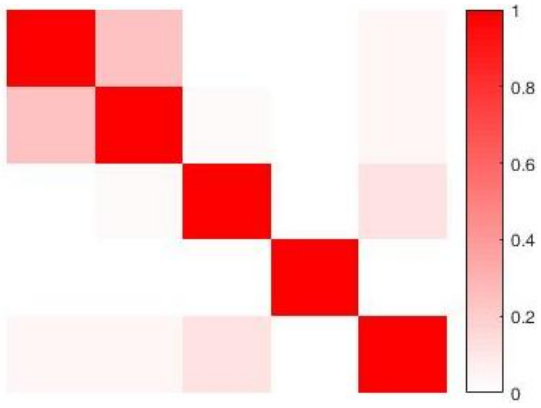


**Figure 6:** *MAC Matrix Graphical Representation*

**Table 11:** *Optimized values for Design Variables*

| Thicknesses (ft.) | | | Concentrated Masses (slugs) | | |
|---|---|---|---|---|---|
| **ID** | **Reference Value** | **Optimized Value** | **ID** | **Reference Value** | **Optimized Value** |
| t1 | 0.0155 | 0.0010 | m1 | 1.9650 | 0.0306 |
| t2 | 0.0006 | 0.00005 | m2 | 1.9650 | 0.0309 |
| t3 | 0.0889 | 0.0056 | m3 | 1.9650 | 0.0310 |
| t4 | 0.0347 | 0.0022 | m4 | 1.9650 | 0.0307 |
| | | | m5 | 0.9825 | 0.0150 |
| | | | m6 | 5.3398 | 0.0835 |
| | | | m7 | 5.3398 | 0.0838 |
| | | | m8 | 5.3398 | 0.0834 |
| | | | m9 | 5.3398 | 0.0828 |
| | | | m10 | 2.6699 | 0.0419 |

### 5.1.2 Sub-case II: $\lambda_L = \frac{1}{9}$

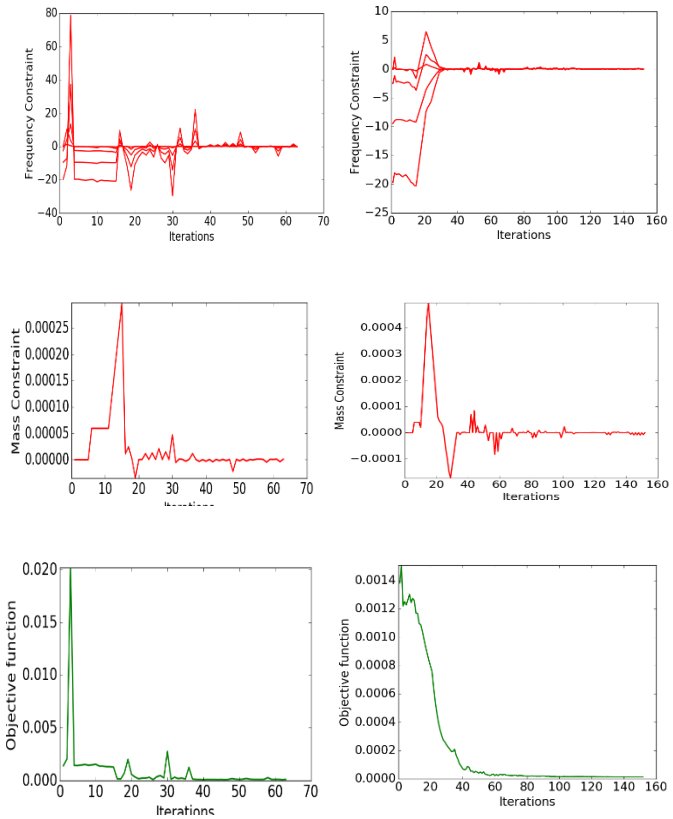


*(a)* *(b)*

**Figure 7:** *Convergence Graphs for (top to bottom) Frequency Constraint, Mass Constraint, and Objective Function; (a) with all bounds normalized together (b) with each bound normalized individually*

**Table 12:** *Modal Response Matching for first 5 modes*

| Mode | Reference Value | Target Value | Optimized Value | Error% |
|---|---|---|---|---|
| **1** | 2.40 | 7.191 | 7.192 | 1e-2 |
| **2** | 8.65 | 25.951 | 25.933 | 7e-2 |
| **3** | 13.22 | 39.667 | 39.665 | 4e-3 |
| **4** | 15.94 | 47.831 | 47.842 | 2e-2 |
| **5** | 24.11 | 72.342 | 72.307 | 4e-2 |
| **Mass (slugs)** | 32.871 | 0.05 | 0.05 | 7e-6 |

$$\begin{bmatrix} 1.00 & 0.24 & 0.00 & 0.00 & 0.05 \\ 0.24 & 1.00 & 0.03 & 0.01 & 0.04 \\ 0.00 & 0.03 & 1.00 & 0.00 & 0.11 \\ 0.00 & 0.01 & 0.00 & 1.00 & 0.00 \\ 0.04 & 0.04 & 0.11 & 0.00 & 1.00 \end{bmatrix}$$

**Matrix 2:** *Modal Assurance Criterion Matrix to ensure Mode Shape matching for first five modes*

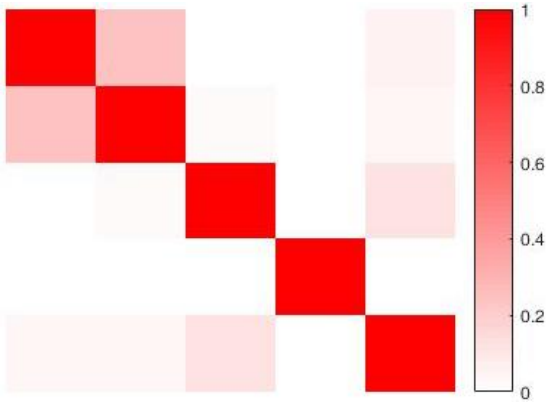


**Figure 8:** *MAC Matrix Graphical Representation*

**Table 13:** *Optimized values for Design Variables*

| Thicknesses (ft.) | | | Concentrated Masses (slugs) | | |
|---|---|---|---|---|---|
| ID | Reference Value | Optimized Value | ID | Reference Value | Optimized Value |
| t1 | 0.0155 | 0.0002 | m1 | 1.9650 | 0.0027 |
| t2 | 0.0006 | 0.00001 | m2 | 1.9650 | 0.0027 |
| t3 | 0.0889 | 0.0011 | m3 | 1.9650 | 0.0027 |
| t4 | 0.0347 | 0.0004 | m4 | 1.9650 | 0.0027 |
| | | | m5 | 0.9825 | 0.0013 |
| | | | m6 | 5.3398 | 0.0073 |
| | | | m7 | 5.3398 | 0.0073 |
| | | | m8 | 5.3398 | 0.0073 |
| | | | m9 | 5.3398 | 0.0073 |
| | | | m10 | 2.6699 | 0.0037 |

### 5.1.3 Sub-case III: $\lambda_L = 4$

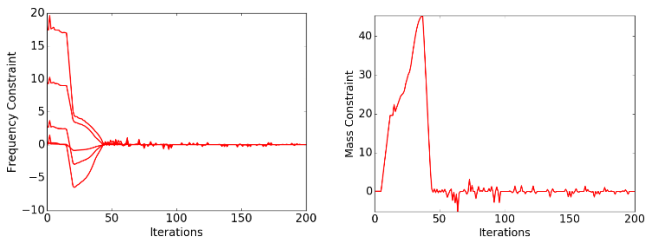


*(a)* *(b)*

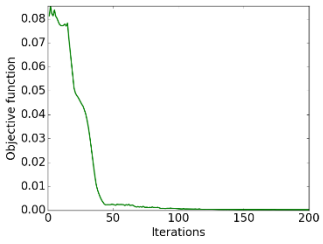


*(c)*

**Figure 9:** *Convergence Graphs (all bounds normalized individually): (a) Frequency Constraint, (b) Mass Constraint, (c) Objective Function*

**Table 14:** *Modal Response Matching for first 5 modes*

| Mode | Reference Value | Target Value | Optimized Value | Error% |
|---|---|---|---|---|
| **1** | 2.40 | 1.199 | 1.199 | 4e-5 |
| **2** | 8.65 | 4.325 | 4.325 | 2e-3 |
| **3** | 13.22 | 6.611 | 6.611 | 2e-4 |
| **4** | 15.94 | 7.972 | 7.972 | 1e-5 |
| **5** | 24.11 | 12.057 | 12.057 | 1e-3 |
| **Mass (slugs)** | 32.871 | 2103.74 | 2103.81 | 3e-5 |

$$\begin{bmatrix} 1.00 & 0.24 & 0.00 & 0.00 & 0.04 \\ 0.24 & 1.00 & 0.02 & 0.01 & 0.03 \\ 0.00 & 0.03 & 1.00 & 0.00 & 0.11 \\ 0.00 & 0.01 & 0.00 & 1.00 & 0.00 \\ 0.04 & 0.04 & 0.11 & 0.00 & 1.00 \end{bmatrix}$$

**Matrix 3:** *Modal Assurance Criterion Matrix to ensure Mode Shape matching for first five modes*

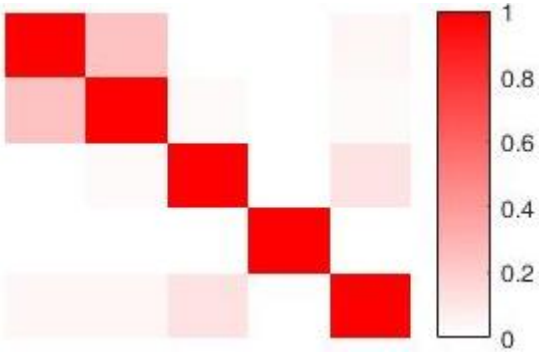


**Figure 10:** *MAC Matrix Graphical Representation*

**Table 15:** *Optimized values for Design Variables*

| Thicknesses (ft.) | | | Concentrated Masses (slugs) | | |
|---|---|---|---|---|---|
| ID | Reference Value | Optimized Value | ID | Reference Value | Optimized Value |
| t1 | 0.0155 | 0.2497 | m1 | 1.9650 | 143.1383 |
| t2 | 0.0006 | 0.0078 | m2 | 1.9650 | 133.9877 |
| t3 | 0.0889 | 1.1739 | m3 | 1.9650 | 105.3963 |
| t4 | 0.0347 | 0.1456 | m4 | 1.9650 | 140.2320 |
| | | | m5 | 0.9825 | 59.1319 |
| | | | m6 | 5.3398 | 331.0407 |
| | | | m7 | 5.3398 | 338.1545 |
| | | | m8 | 5.3398 | 338.6400 |
| | | | m9 | 5.3398 | 346.9379 |
| | | | m10 | 2.6699 | 167.0664 |

## 5.2 GARTEUR SM-AG19

### 5.2.1 Sub-case I: $\lambda_L = \frac{1}{9}$

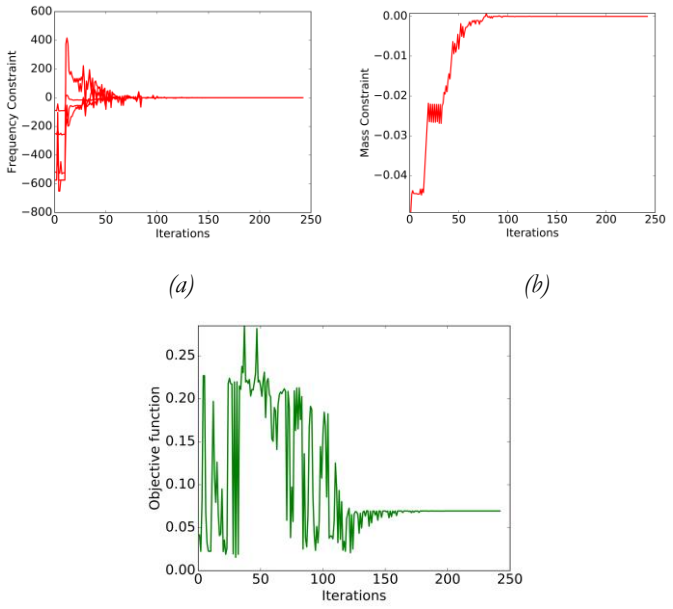


*(a)* *(b)* *(c)*

**Figure 11:** *Convergence Graphs (all bounds normalized individually): (a) Frequency Constraint, (b) Mass Constraint, (c) Objective Function*

**Table 16:** *Modal Response Matching for first 5 modes*

| Mode | Reference Value | Target Value | Optimized Value | Error% |
|---|---|---|---|---|
| **1** | 6.37 | 19.100 | 19.100 | 0e+0 |
| **2** | 17.32 | 51.955 | 51.955 | 0e+0 |
| **3** | 39.37 | 118.098 | 118.098 | 2e-5 |
| **4** | 46.02 | 138.045 | 138.045 | 7e-6 |
| **5** | 46.08 | 138.243 | 138.243 | 2e-5 |
| **Mass (kg)** | 41.2650 | 0.0566 | 0.0566 | 2e-8 |

$$\begin{bmatrix} 0.99 & 0.00 & 0.00 & 0.00 & 0.00 \\ 0.00 & 0.97 & 0.01 & 0.00 & 0.00 \\ 0.00 & 0.02 & 0.93 & 0.00 & 0.00 \\ 0.00 & 0.00 & 0.00 & 0.88 & 0.12 \\ 0.00 & 0.00 & 0.00 & 0.12 & 0.88 \end{bmatrix}$$

**Matrix 4:** *Modal Assurance Criterion Matrix to ensure Mode Shape matching for first five modes*

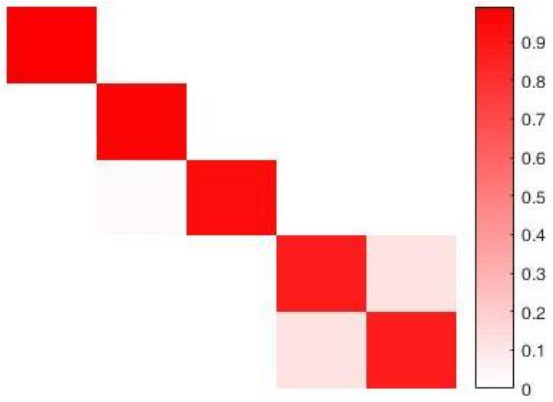

**Figure 12:** *MAC Matrix Graphical Representation*

**Table 17:** *Optimized values for Design Variables*

| Thicknesses (mm) | | | Concentrated Masses (kg) | | |
|---|---|---|---|---|---|
| ID | Reference Value | Optimized Value | ID | Reference Value | Optimized Value |
| t1 | 50 | 6.4676 | m1 | 0.5 | 0.0007 |
| t2 | 11 | 0.5277 | m2 | 0.2 | 0.0003 |
| t3 | 10 | 0.8824 | m3 | 0.2 | 0.0003 |
| t4 | 10 | 0.8842 | | | |
| t5 | 10 | 0.3919 | | | |
| t6 | 10 | 0.4347 | | | |

### 5.2.2 Sub-case II: $\lambda_L = 2$

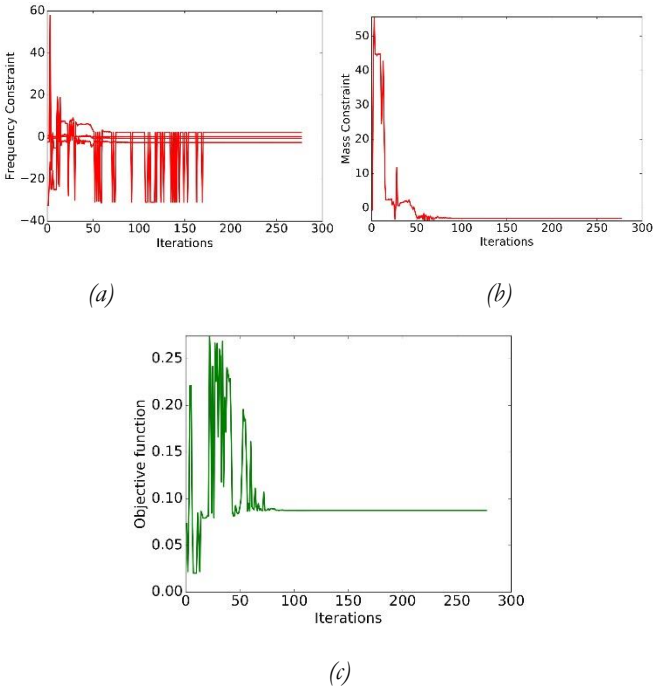


*(a)* *(b)* *(c)*

**Figure 13:** *Convergence Graphs (all bounds normalized individually): (a) Frequency Constraint, (b) Mass Constraint, (c) Objective Function*

**Table 18:** *Modal Response Matching for first 5 modes*

| Mode | Reference Value | Target Value | Optimized Value | Error% |
|---|---|---|---|---|
| **1** | 6.37 | 4.548 | 4.584 | 8e-1 |
| **2** | 17.32 | 12.370 | 12.279 | 7e-1 |
| **3** | 39.37 | 28.119 | 23.175 | 1.7e+1 |
| **4** | 46.02 | 32.868 | 28.473 | 1.3e+1 |
| **5** | 46.08 | 32.915 | 30.625 | 6.9e+1 |
| **Mass (kg)** | 41.2650 | 330.12 | 327.15 | 8.9e-1 |

$$\begin{bmatrix} 0.99 & 0.00 & 0.00 & 0.00 & 0.00 \\ 0.00 & 0.98 & 0.01 & 0.00 & 0.00 \\ 0.00 & 0.02 & 0.57 & 0.00 & 0.00 \\ 0.00 & 0.00 & 0.00 & 0.99 & 0.12 \\ 0.00 & 0.00 & 0.00 & 0.12 & 0.99 \end{bmatrix}$$

**Matrix 5:** *Modal Assurance Criterion Matrix to ensure Mode Shape matching for first five modes*

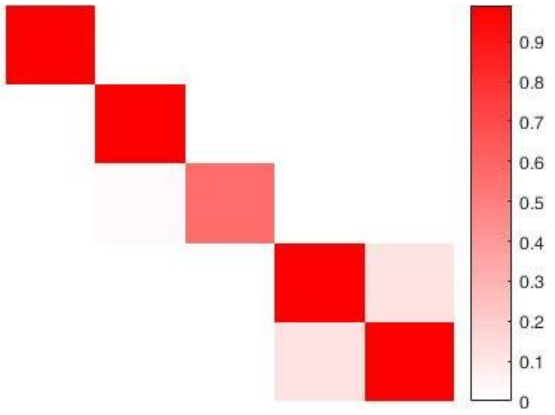

**Figure 14:** *MAC Matrix Graphical Representation*

**Table 19:** *Optimized values for Design Variables*

| Thicknesses (mm) | | | Concentrated Masses (kg) | | |
|---|---|---|---|---|---|
| **ID** | **Reference Value** | **Optimized Value** | **ID** | **Reference Value** | **Optimized Value** |
| t1 | 50 | 90 | m1 | 0.5 | 4 |
| t2 | 11 | 30 | m2 | 0.2 | 1.6 |
| t3 | 10 | 24 | m3 | 0.2 | 1.6 |
| t4 | 10 | 24 | | | |
| t5 | 10 | 24 | | | |
| t6 | 10 | 24 | | | |

## 6 Multidisciplinary Analysis & Optimization

To perform aeroelastic optimization it is necessary to have a tool that is capable of carrying out a structural analysis, in order to determine the extent of the structural deformations as well as the stresses generated in the structure under the action of the aerodynamic loads. Therefore, this tool should also be capable of performing aerodynamic analysis, in order to determine the aerodynamic forces as a function of the flight variables, able to perform a dynamic analysis and determine factors such as flutter velocity, frequency and damping depending on variables such as flight velocity. After we have a tool, which is capable of performing structural and aerodynamic analysis, we need a tool to optimize the problem, by modifying the design variables to obtain an optimized solution that is characterized by the minimum value of the objective function of the optimization problem.

We adapt an optimization methodology [1] that is described in **Figure 15.**

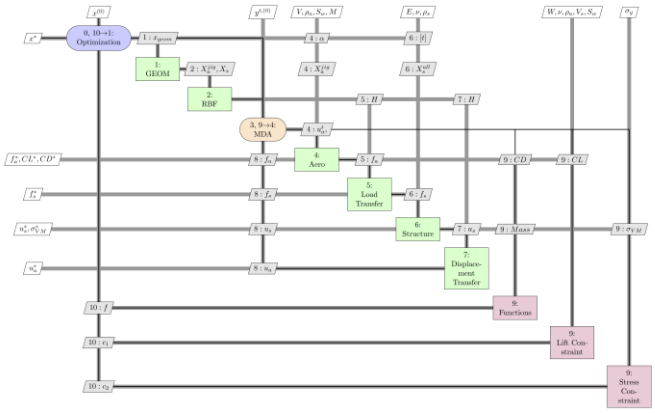


**Figure 15:** *XDSM Diagram of the Multi-disciplinary Analysis and Optimization Process* [1]

The steps that define the optimization process are the following:

0. Initiation of Optimization process
1. The initial geometry is created.
2. The interpolation matrix to couple aerodynamic and structure is created.
3. Initiation of coupling process between aerodynamic forces and structural displacements.
4. Determination of the aerodynamic loads by aerodynamic analysis.
5. Transfer of aerodynamic loads from aerodynamic mesh to structural mesh.
6. Determination of the structural displacements and stresses.
7. Transfer of structural displacements from structural mesh to aerodynamic mesh.
8. Determination of the characteristics of the wing for this configuration.
9. Computation of the constraints.
10. Based on the objective function and constraints value, design variable values are given for next optimization iteration.

Steps 1 to 10 are repeated until the defined convergence is achieved.

A modification to this XDSM diagram is viewed, which is to put 1 and 2 out of the optimization loop 0, as our task here does not include the change in geometry and Radial Based Functions (RBF).

## 6.1 Description of Components of XDSM Diagram

1. **Geometry (GEOM):** It creates the initial geometry from the parameters specified in the main definition of the structure observed.
2. **RBF:** In general, the structural and aerodynamic grids are not coincident. RBF creates the interpolation matrix to couple the aerodynamic and structure components. Once the interpolation matrix **H** is created, it can stored and used for the whole optimization process, as the dimensions of the problem do not change. (That is the reason why it can be put outside the optimization loop).
3. **Aerodynamics:** This component performs an aerodynamic analysis using the external software, extract the aerodynamic characteristics of the wing, and stores it for each iteration. The aerodynamic loads are computed with a **Potential Flow Panel Code, Panair/A502**, which determines the value of pressure coefficient $C_p$ at the control points of the panel, given the angle of attack, and the Mach number. The result from this component are the aerodynamic loads for each grid point for each iteration.
4. **Load Transfer:** The aerodynamic loads are transferred from aerodynamic mesh to structural mesh with the help of a transformation matrix.
5. **Structure:** This component uses Nastran95 to perform static, modal and/or dynamic analysis of the wing. The load transfer is performed from aerodynamic mesh to structure mesh. Now the structural loads are used to produce displacement deformations and Von mises stresses.
6. **Displacement Transfer:** The deformations recorded by the Structure component are now transferred to the aerodynamic grid using a displacement interpolation matrix.

## 6.2 Objective Function and Constraints

The primary thoughts on the objective function is to minimize the coefficient of induced drag $C_{D_i}$ and structural mass $W$.

$$F = \alpha C_{D_i} + \beta W \tag{26}$$

Where $\alpha$ and $\beta$ are scalar parameters that is indicative of the relative importance of the variables that we want to minimize.

The constraints would concern the lift, where the lift must be at least as much as the structural weight $W$ during the cruise. We can constrain $C_L$ by periodically adjusting of the angle of attack of the aircraft within the aero-structural solution until the desired lift is obtained. The stress constraint can also put which will make sure that the stress in the material is lower than the yield stress at various load condition.

## 7 Blended Wing Body Characteristics

The Blended Wing Body (hereafter abbreviated as BWB) is a new concept aircraft for which various departments of ISAE-SUPAERO are working together. **Figure 16** shows the BWB aerodynamic model and **Table 20** depicts the dimensional data.

The airfoil data and dimensional data such as span, chord lengths, sweeps, and relative positions of airfoils are manually extracted and calculated from the VSP file of BWB aerodynamic model. This task is quite hefty as to align with an existing VSP code, and extracting particular data is not trivial.

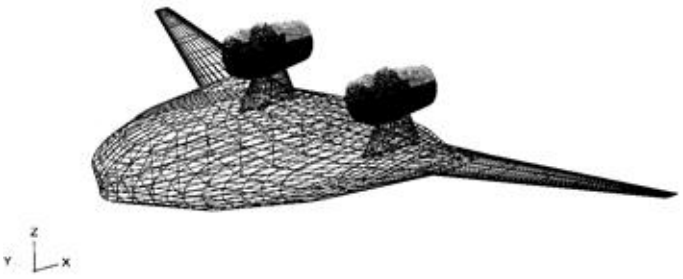

**Figure 16:** *Blended Wing Body Aerodynamic Model**

*This aerodynamic model is as a result of Claudia Bruni's code, later improved by Alessandro Sgueglia. The VSP code was accessed to extract the required information for this work.

**Table 20:** *Characteristics of the Half-span BWB Aerodynamic Model (units - m)*

| Airfoil | Root C | Dist. from Sym Plane | Sweep at LE | Sweep to $X_{le}$ |
|---|---|---|---|---|
| **1** | 20 | 0 | 35.41° | 0 |
| **2** | 16.91 | 3.68 | 60° | 2.61 |
| **3** | 11.5 | 6.26 | 40°(0.75C) | 7.08 |
| **4** | 4.30 | 9.03 | 30° | 14.81 |
| **5** | 0.91 | 20.57 | - | 21.66 |

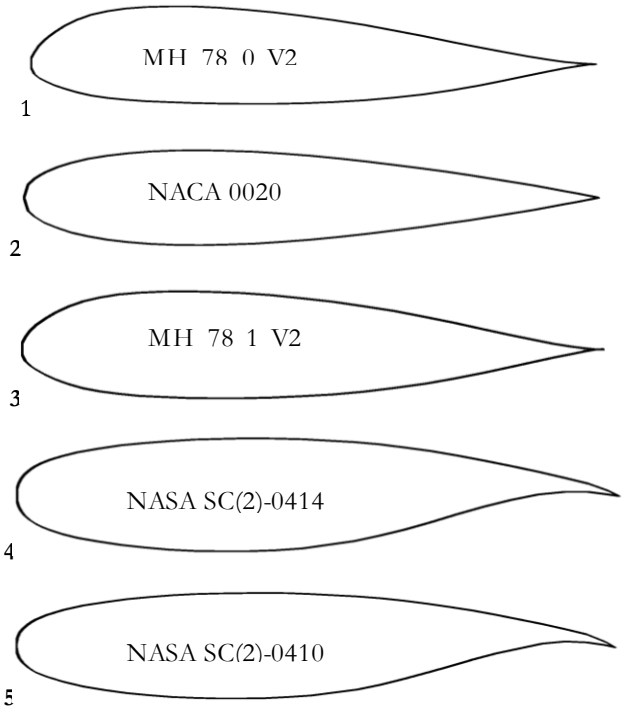


**Figure 17:** *Airfoil Profiles from Root-to-Tip of the Wing (1 -5)*

The airfoil profiles in **Figure 17** are generated by performing the following procedure:

1. Manually extracting coordinates from VSP code
2. Performing linear interpolation with a python code on the coordinates to have uniform X coordinates for both upper and lower Y coordinates
3. Operating on airfoil coordinates to get the same number of points for all the airfoils

Once the final coordinates are saved, the section of wing is studied in VSP GUI, followed at the same time with VSP code. The section spans, sweeps, and chord lengths are

operated upon to get sufficient data for the next step. Some of the data is depicted in **Table 20.**

## 8 Aerodynamic Mesh Generation

The wing is generated with the data as mentioned in Section 7. The python script written by Mas Colomer [1] is kept as a base and improved upon to get the geometry of the wing as per our requirements.

The existing python script was only capable of generating a wing geometry with same airfoil throughout the span of the wing. The 'airfoil' data was given as a global variable, and therefore, the exact code could not work for this work. As a part of this work, we upgraded this script to incorporate different airfoil profiles for each section of the wing. The python script now can generate any wing geometry, provided with the information in the input XML file. This is one of the novelties added to the existing project, with this work.

The wing section information as calculated in Section 7 are parsed in the XML file which in itself calls the airfoil data for each section, stored in text files.

As a result of compilation of the script, a geometry and a mesh is generated and can be visualized using **Gmsh** or a similar software. **Figure 18** shows the wing model generated with this script.

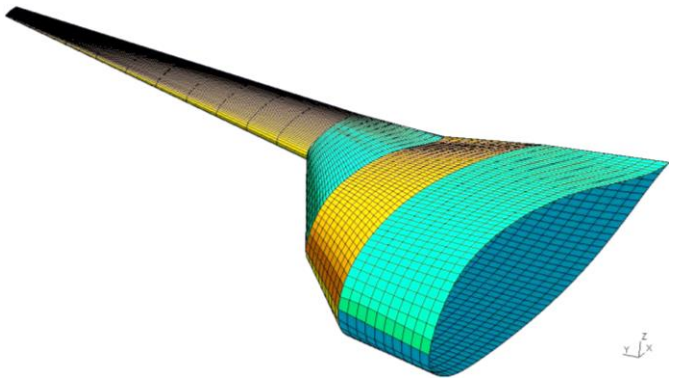

**Figure 18:** *Half-span BWB Aerodynamic Mesh reproduced with the Python Script*

## 9 Finite Element Mesh Generation

The next step after generating an aerodynamic model mesh is to generate a finite element mesh. The structural wing box does not have to be in a perfect wing profile so far it matches the shape of the wing. The structural wing geometry generation is not a part of this work, however, after several tries to rectify the provided geometry, we opted to create the structural model from scratch and mesh it. **Figure 19** shows the wing model geometry created in MSC Patran with exact dimensions as of the aerodynamic model. However, the material properties, and thicknesses are still unknown.

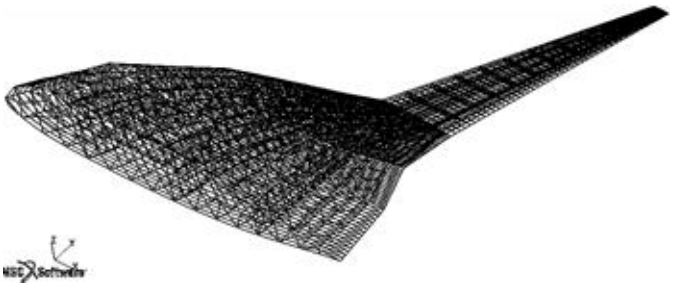

**Figure 19:** *Half-span BWB FEM Mesh generated with MSC Patran*

## 10 Future Works

Due to limited time and organizational problems to get required data for this work, the aimed result is not achieved. The next steps in this works would be as follows:

1. Getting the material data and thicknesses for finite element mesh model
2. Preparing the structure model and the aerodynamic model for the MDA using Panair, as mentioned in the Github tutorial of Mas Colomer [1]
3. Perfoming the MDA with proposed methodology (Figure 15)
4. Aeroelastic scaling of the BWB
5. Flutter analysis & optimization within MDO

The perspective of this project would be to learn the theory of dynamic aeroelastic scaling, perform dynamic modal optimization of the BWB for scales greater and smaller than one, and flutter analysis and optimization for the reference BWB. In this part of the work, there would be no flow similarity assumption, hence, it will an integral part of the work to maintain structure and aerodynamics in place. The flutter optimization will be performed for scaled models of scales both greater and smaller than one. In the end, a research paper will be published with new findings and improvements on existing concepts, as seen throughout the course of this work

## 11 Conclusions

Aeroelastic scaling is a complex task but if performed well, it can produce good results that are comparable for a full scale model. In this work, we mainly focused on aeroelastic scaling and modal response optimization for two test cases which were further divided into three and two sub-cases, respectively. The whole process of scaling and optimization requires thorough understanding of the theory, and proficient use of the optimization tools.

For the first test case, i.e., GOLAND wing, the results are extremely good. The scaled model almost completely duplicates the modal behavior of the reference full scale model. The frequencies and the masses of all the three sub-cases matches almost completely to the target frequencies and masses of their respective theoretical target values. An average error of 0.001% is observed.

In Section 5.1.2, a comparison of convergence is made between the optimization carried out with same bound normalization for all design variables, and with individual bound normalization for all design variables depending on their initial value. It can be observed that with individual normalization, we achieve convergence in a much smoother manner, however it takes some extra iterations. For all the cases discussed after Section 5.1.2, individual normalization of bound of design variables is used. It is a necessity as well as a preference.

For the GARTEUR SM-AG19 model, which is a more complicated model as compared to the GOLAND wing, the results are up-to the expectations. Several intermediate iterations were performed and it was found out that the tolerance of the optimizer played a big role in the convergence of objective function. For the *sub-case I*, the tolerance was decreased $10^5$ times (from default of 1e-3 to 1e-8) to achieve good results. For *sub-case II,* the tolerance was decreased $10^{12}$ times (from default of 1e-3 to 1e-15).The scaled models for both the test cases closely duplicate the behavior which was expected in theory. For the second test sub-case, four out of five modes match with the reference model perfectly. It is still under improvement, however, the frequencies and mass has converged close to target values. The way to correct that could be to increase the total number of modes extracted M, or start from a completely different starting point of design variables in order to avoid a possible local optima problem.

The main contributions to the scaling tool developed by Mas Colomer et al. [1] can be listed as follows:

- Use of tools for scales both greater and smaller than one
- Use of preliminary rule to estimate the scaled baseline design so as not to start from a completely blind point
- Exposing the problematics of local modes, as low frequency modes fill most of the available space for the mode comparison, if the design space is too large
- Exhibiting importance of individual normalization for each design variable to:
    1. Constrain the design space to avoid the generation of local modes
    2. Avoid dipping of the COBYLA optimizer in the negative values of the design variables which has no physical sense, and hence produces fatal error in Nastran analysis

The main contribution to the geometry and mesh generating python script is to upgrade it to incorporate different airfoils and generate any kind of wing.

The BWB aerodynamic model and structure model are both reproduced correctly. The next steps as mentioned in Section 10 are to be followed in order to complete this project.

## 12 References

[1] Joan Mas Colomer, Nathalie Bartoli, Thierry Lefebvre, Sylvian Dubreuil, Joaquim R.R.A. Martins, Emmanuel Benard, and Joseph Morlier. ONERA, and ISAE. Similarity Maximization of a Scaled Aeroelastic Flight Demonstrator via Multidisciplinary Optimization, AIAA (2017).

[2] E. Buckingham. On physically similar systems; Illustrations of the use of dimensional equations. Physical Review, 4(4):345–376, 1914.

[3] Raymond L. Bisplinghoff and Holt Ashley. Principles of Aeroelasticity. General Publishing Company, Ltd., 895 Don Mills Road, Toronto, Ontario, 1962.

[4] C. H. Wolowicz, J. S. Bowman, and W. P. Gilbert. Similitude requirements and scaling relationships as applied to model testing. NASA Technical Paper, (1435), 1979.

[5] P. Pereira, L. Almeida, A. Suleman, V. Bond, R. A. Canfield, and M. Blair. Aeroelastic Scaling and Optimization of a Joined-Wing Aircraft Concept. PhD thesis, 48th AIAA/ASME/ASCE/AHS/ASC

Structures, Structural Dynamics, and Materials Conference, 2007.

[6] Jenner Richards, Afzal Suleman, Tyler Aarons, and Robert Canfield. Multidisciplinary design for flight test of a scaled Joined Wing SensorCraft. Multidisciplinary Analysis Optimization Conferences (AIAA), Fort Worth, 2010.

[7] Charles A.G. Eger. Design of a scaled flight test vehicle including linear aeroelastic effects. Master's thesis, Virginia Polytechnic Institute and State University, Blacksburg, U.S.A., 2013.

[8] Charles Eger, Anthony Ricciardi, Robert, and Mayuresh Patil. Design of a scaled flight test vehicle including linear aeroelastic effects. 54th AIAA/ASME/ASCE/AHS/ASC Structures, Structural Dynamics, and Material Conference Paper, 2013.

[9] Vanessa L. Bond, Robert A. Canfield, Afzal Suleman, and Maxwell Blair. Aeroelastic scaling of a joined wing for nonlinear geometric stiffness. AIAA journal, 50(3):513–522, 2012.

[10] Anthony P. Ricciardi. Geometrically Nonlinear Aeroelastic Scaling. PhD thesis, Faculty of the Virginia Polytechnic Institute and State University, 2013.

[11] Ricciardi et al. (2014), Nonlinear Aeroelastic-Scaled-Model Optimization Using Equivalent Static Loads.

[12] Tiago José Fernandes Pires, Linear Aeroelastic Scaling of a Joined Wing Aircraft, Master Thesis, Técnico Lisboa, July 2014.

[13] Anthony P. Ricciardi, Robert A. Canfield, Mayuresh J. Patil, and Ned Lindsley. DOI:10.2514/1.C033171. Nonlinear Aeroelastic Scaled-Model Design. Journal of Aircraft (2016).

[14] Girard, A. and Roy, N., Structural dynamics in industry, Wiley, 2008.

[15] Link, M. and Friswell, M., "Working Group 1: Generation of Validated Structural Dynamic Models-Results of a Benchmark Study Utilising the GARTEUR SM-AG19 Testbed," Mechanical Systems and Signal Processing, Vol. 17, No. 1, Jan. 2003, pp. 9-20

## 13 Appendix: Finding Similarity Parameters

It is important to understand how the similarity parameters can be found. **Figure 10** and **11** shows a reference full scale model and a scaled model (respectively) of a deflected cantilever beam.

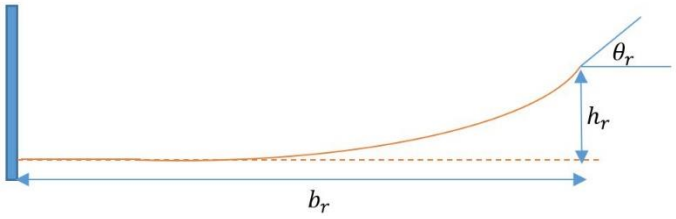


**Figure 15: Reference full scale model**

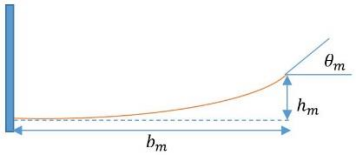


**Figure 16: Scaled model**

To find a similarity parameter between the two models, we follow the formulation as stated below:

We know that, $\theta_r = \theta_m$

$h_r \neq h_m$

Writing it in a vector form,

$$x_r = \begin{Bmatrix} h_r \\ \theta_r \end{Bmatrix} \qquad x_m = \begin{Bmatrix} h_m \\ \theta_m \end{Bmatrix}$$

Normalizing the vectors,

$$\bar{x}_r = \begin{Bmatrix} \frac{h_r}{b_r} \\ \theta_r \end{Bmatrix} \qquad \bar{x}_m = \begin{Bmatrix} \frac{h_m}{b_m} \\ \theta_m \end{Bmatrix}$$

If similarity exists, then,

$$\bar{x}_r = \bar{x}_m$$

Hence, we have found one similarity parameter between these two models.